Eidgenössische Technische Hochschule Zürich
Swiss Federal Institute of Technology Zurich

Institut für
Technische Informatik und
Kommunikationsnetze

# Analytical model for indoor solar energy harvesting

Bachelor Thesis

Alexandra Schneider
aleschne@ethz.ch

Computer Engineering and Networks Laboratory
Department of Information Technology and Electrical Engineering
ETH Zürich

**Supervisors:**
Naomi Stricker
Stefan Drašković
Prof. Dr. Lothar Thiele

July 5, 2021

# Acknowledgements

I would like to express my deep gratitude to Prof. Dr. Lothar Thiele for giving me the opportunity to write this interesting bachelor thesis at the Computer Engineering Group at ETH Zurich. My sincere gratitude is extended to my supervisors Naomi Stricker and Stefan Drašković. Their valuable feedback and constant, generous support have made this thesis a very enjoyable an fruitful experience. Finally, I want to thank my family for their endless support throughout my studies and bachelor thesis.

# Abstract

For many indoor deployed internet of things (IoT) nodes, solar energy harvesting provides a sustainable and autonomous energy source. However, as indoor solar panels can harvest only around 0.1 % of the energy that a panel would otherwise harvest outdoors, reliable models are required to realize the untapped potential of this energy source. Such models should be able to accurately estimate the amount of energy that can be harvested over a given time horizon. Such knowledge can be used to predict future harvestable energy, dimension a system, or determine where a solar device should be placed to maximize its energy harvesting.

In this bachelor thesis, an analytical model is developed to calculate the amount of harvestable energy at any indoor location originating from natural light sources. It consists of two submodels, namely an illuminance and an energy model. The illuminance model converts outdoor irradiance measurements into an interior illuminance distribution and the energy model converts indoor illuminance into harvestable energy. Two parts of the analytical model are evaluated through a real-world data set. Furthermore, this bachelor thesis evaluates the deployment of indoor solar harvesting devices. The deployment model characterizes potential device positions based on the number of direct sunlight hours and is also assessed through real-world data.

# Contents

Chapter 1

# Introduction

Solar energy devices can be deployed at any light exposed location with no infrastructure costs, while working autonomously and providing energy for internet of things (IoT) nodes in a sustainable fashion. However, indoor-deployed devices often have small rechargeable energy storages such as supercapacitors, making them sensitive to a variable and unpredictable environment. Furthermore, indoor solar panels can harvest only around 0.1 % of the energy that a panel would harvest outdoors.

To realize the unexploited potential of indoor solar harvesting, reliable models are needed which can provide guidance in the dimensioning and deployment of indoor energy harvesting systems.

In this work, an analytical model is developed which determines the amount of harvestable energy at indoor locations, originating from natural light sources. It consists of two submodels, an illuminance and an energy model. The illuminance model converts irradiance measurements into an interior illuminance distribution which considers the room and window geometries. The energy model translates the interior illuminance distribution into harvestable energy. In addition to the analytical model, this work considers the deployment of indoor solar harvesting devices. Using previous models and conclusions from the analytical model, the direct sunlight hour distribution inside a specific location at ETH Zurich is evaluated.

While other studies [1] [2] [3] have focused on developing interior illuminance models, this work deals with the extension of an illuminance model to a full analytical model which translates outdoor irradiance measurements into interior harvestable energy. Therefore, the conversion of illuminance to energy is considered, in the interest of offering an accurate estimation on how much energy can be harvested at an indoor location.

Through the development and evaluation of an analytical model, this work arrives at several conclusions regarding indoor solar energy harvesting. On the one hand, the evaluation of the beam illuminance model verifies a high correlation between a beam illuminance condition and measured illuminance peaks. On the other hand, the assessment of the energy model performance results in

the observation of varying accuracy between the two evaluated locations. While performing well in both cases, the model tends to underestimate the harvestable energy at the energy peaks in the location which harvests generally more energy. Another conclusion, that can be drawn from the energy model, is that in order to harvest more energy the solar panel size can be increased or that the solar panel's placement should be adjusted to ensure maximum exposure to direct sunlight.

The deployment model evaluation, which assesses whether the condition for direct sunlight is fulfilled for a grid of points, arrives at multiple findings regarding ideal solar panel placement. In the considered location at ETH Zurich, three different potential solar panel deployment heights and two walls are evaluated. In terms of the different heights, it is observed that more energy can be harvested when the solar panel is placed near the window. However, the amount of beam illuminance hours can vary greatly around the window itself. Furthermore, a shift of the beam illuminance hour distribution according to the sun movement can be seen. This shift is also observed in the evaluation of the two walls. However, the positions with the largest number of beam illuminance hours are not found in the area closest to the window anymore. Through the sun movement, the highest number of beam illuminance hours are shifted slightly away from the window. As the sun movement varies not only over the day but also over the whole year, the placement of a solar harvesting device has to be adjusted over time to continue capturing the maximum amount of energy.

The remainder of this work is structured as follows: The reader is introduced to the terminology and related work in Chapter 2. Then, in Chapter 3, the analytical model is presented. On one hand, the illuminance model is explained, and on the other hand, the energy model and its derivation are discussed. Chapter 4 deals with the evaluation of the beam illuminance and energy model. In Chapter 5, the deployment model and its evaluation are discussed. After providing an outlook on future work in Chapter 6, the report summarizes the main conclusion in Chapter 7.

Chapter 2

# Background

This chapter offers a summary of the used terminology and previous work relevant for the project.

## 2.1 Terminology

**Solar radiation**
Solar radiation is electromagnetic energy originating from the sun. Its spectrum can be split into ultraviolet, infrared and visible light bands. These three spectral bands constitute approximately 8%, 50% and 42% respectively of the light that reaches the earth's surface [4]. The amount and intensity of solar radiation that a location receives depends on a variety of factors such as latitude, altitude, season, time of day and cloud cover [4].

**Irradiation** $H$
Irradiation is the process by which an object is exposed to radiation. In this paper the exposure originates from the sun. Its SI unit is kilo watt hour per square meter ($kWh/m^2$). The overall global irradiation $H$ is composed of two components, beam $H_b$ and diffuse irradiation $H_d$ [3].

**Irradiance** $E_e$
Irradiance is the radiant flux $\Phi_e$ received by a surface $A$:

$$E_e = \frac{\partial \Phi_e}{\partial A}$$

Its SI unit is watt per square meter ($Wm^{-2}$). The overall global irradiance $E_e$ is composed of two components, beam $E_{e,b}$ and diffuse irradiance $E_{e,d}$ [3].

**Illuminance** $E_v$
Illuminance is the total luminous flux $\Phi_v$ incident on a surface $A$, per unit area:

$$E_v = \frac{\partial \Phi_v}{\partial A}$$

It is a measure of how much the incident light illuminates the surface, wavelength-weighted by the luminosity function to correlate with the human eye's brightness perception [5]. Its SI unit is lux ($lx$), or equivalently lumens per square meter ($lm\ m^{-2}$). The total illuminance $E_v$ is composed of three components, diffuse $E_{r,d}$, beam $E_{r,b}$ and reflected illuminance $E_{r,r}$ [3].

**Luminous flux $\Phi_v$**
Luminous flux is the measure of the perceived power of light. In contrast to radiant flux, it is adjusted to reflect the sensitivity of the human eye which varies according to the received wavelength [5]. The adjustment is done by weighting the power at each wavelength with the luminosity function [5]. The SI unit of luminous flux is the lumen ($lm$).
The following equation calculates the total luminous flux $\Phi_v$ in a source of light through the photopic luminosity function:

$$\Phi_v = 683.002(lm/W) \int_0^\infty V(\lambda)\Phi_{e,\lambda}(\lambda)\, d\lambda$$

with $\Phi_{e,\lambda}$ being the spectral radiant flux, in watts per manometer, $V(\lambda)$ being the luminosity function and $\lambda$ being wavelength, in nanometers.

**Luminosity function $V(\lambda)$**
The CIE photopic luminosity function $V(\lambda)$ is a standard function established by the Commission Internationale de l'Éclairage (CIE) and can be used to convert radiant energy into luminous energy [6]. It describes the human eye's response to different wavelengths.

**Radiant flux $\Phi_e$**
In radiometry, radiant flux or radiant power is the measure of the total power of electromagnetic radiation or the radiant energy emitted or received, per unit time:

$$\Phi_e = \frac{\partial Q_e}{\partial t}$$

where $Q_e$ is the radiant energy emitted or received over time $t$. The SI unit of radiant flux is Watt ($W$).

**Luminous efficacy of radiation $K$**
Luminous efficacy of radiation measures the fraction of electromagnetic power usable for lighting, measured in lumens per watt ($lm/W$). It is obtained by dividing the luminous flux by the radiant flux [5]:

$$K = \frac{\Phi_v}{\Phi_e}$$

For monochromatic light at a wavelength of $555nm$, the photopic luminous efficacy of radiation has a maximum possible value of 683.002 $lm/W$ [5].

## 2.2 Related work

Several existing publications were considered and leveraged for this work. [1] presents a systematic approach to offline capacity planning of a power subsystem for solar energy harvesting systems. The approach is based on a modified astronomical model and considers seasonal variations of the energy source. The results show that pre-deployment design considerations are important for achieving long-term reliable system operation. Developing an analytical model for indoor solar energy harvesting, as presented in this work, allows the same considerations to be done for an indoor environment.
[3] introduces the simulation tool DeLight which uses as input data hourly horizontal beam and diffuse irradiance measurements, which are readily available at many weather stations around the world. It is explained how to convert irradiance measurements into indoor illuminance, and the performance of the model is evaluated for several luminous efficacy and sky luminance models. In this work, the illuminance model is part of the analytical model which computes the harvestable energy indoors.
Additional related studies are provided by [7], [2] and [8]. [7] assesses the correlations of global and diffuse solar luminous efficacy for all sky conditions. [2] presents an algorithm framework for sky luminance distribution, based on theoretical considerations of the CIE general model, in order to accurately predict indoor illuminance. [8] compares three well-known sky distribution models with measured data.
Related work on interior energy harvesting can be found in [9]. The estimation of harvestable energy in time-varying indoor light conditions is addressed and the influence of considering spectral information on the energy estimation accuracy is evaluated. The results of the article show that a spectrum-based method leads to significant performance improvements in cases where the light condition is not defined by a single light source which is the situation for this work. [6] proposes a new luminosity function, that improves upon the original CIE 1924 function which is generally used in terms of illuminance to intensity conversion.

Chapter 3

# Analytical model

In this chapter, the analytical model for indoor solar energy harvesting is introduced. It combines an illuminance and energy model. Both submodels are discussed and the derivation of the energy model is explained.

## 3.1 Analytical model

The analytical model is the combination of an existing model for interior illuminance distribution and a newly derived model for energy calculation. The illuminance model converts irradiance measurements into illuminance values. The energy model takes the output of the illuminance model as an input and converts it into harvestable energy.
In Figure 3.1, the analytical model with its two submodels is shown. The analytical model takes hourly horizontal global and diffuse irradiance measurements as well as the room and window geometries as an input. Through the illuminance model, which consists of a sky luminance, luminous efficacy, and interior light transfer model, these are converted into an interior illuminance distribution. In a next step, the energy model computes the luminous and radiant flux based on the interior illuminance distribution. The output of the analytical model is the interior energy distribution.

## 3.2 Illuminance model

In this section, the interior light transfer model and its components are discussed. Furthermore, the conditions for direct sunlight are introduced.

Generally, the DeLight Algorithm takes the global horizontal and diffuse irradiance measurement as an input, which can be computed from solar radiation measurements [3]. The total irradiance $G_i$ is the sum of the beam irradiance $G_{bi}$, the diffuse irradiance $G_{di}$, and the reflected irradiance $G_{ri}$ [3]. To convert

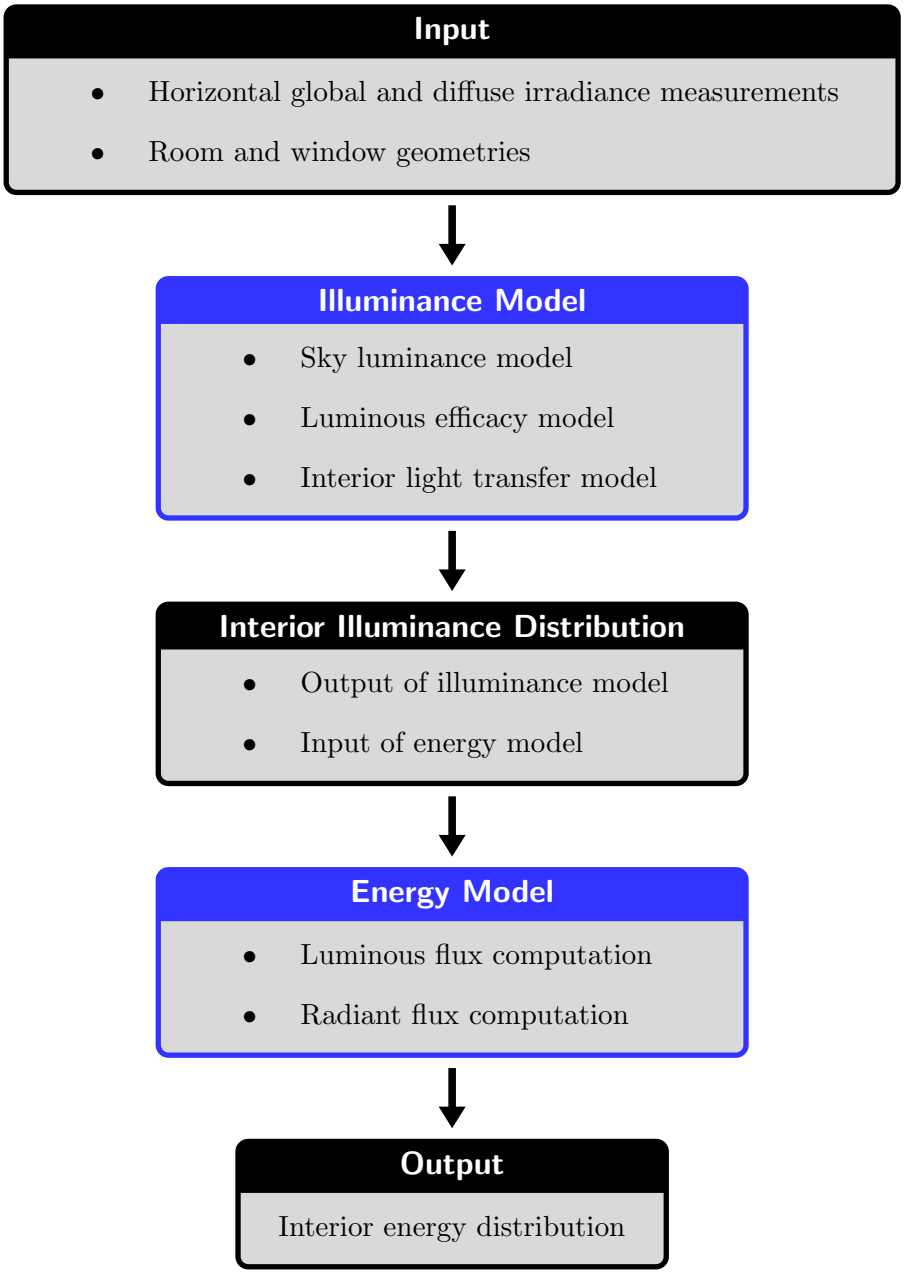


Figure 3.1: Schematic diagram of the analytical model

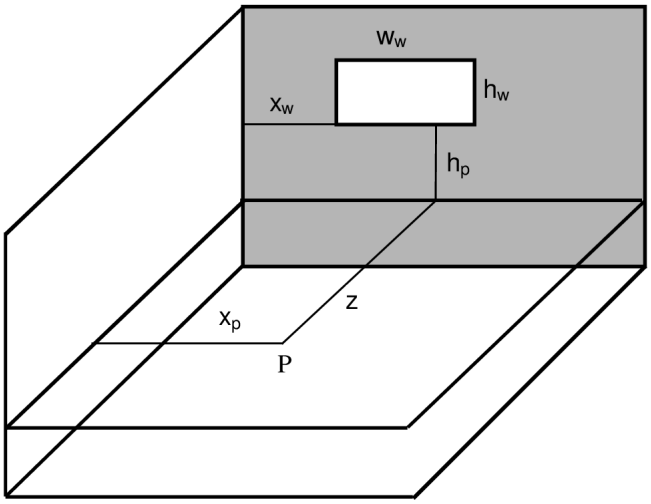


Figure 3.2: Selected room and window geometry considered in analytical model (illustration from [3])

the solar irradiance measurements into illuminance values, a luminous efficacy model is applied. Several luminous efficacy models exist which vary in the accuracy of their performance. The luminance value of each point in the sky is usually calculated by a sky luminance model, taking the horizontal beam and diffuse illuminance values as an input. As in the case of luminous efficacy, there are several models to choose from. The interior light transfer model determines the illuminance distribution inside a room, while taking into consideration the geometry of the room, such as the width of the room or the size of the window. Some of the considered room and window geometries are shown in Figure 3.2 [3]. The total illuminance $E_v$ consists of the three components, beam illuminance $E_{r,b}$, diffuse illuminance $E_{r,d}$ and reflected illuminance $E_{r,r}$ [3].

The exposure of a point P to beam illuminance is tied to the condition that the sun is directly visible at that place. To assess whether this is the case, the following two inequations need to be fulfilled:

$$\theta_1 < \theta_s < \theta_2 \quad \text{and} \quad \psi_1 < \psi_{sw} < \psi_2$$

- $\theta_1$ and $\theta_2$ are the altitude angle of the lower, respectively the upper edge of the window relative to the point of reference P (in radians)
- $\psi_1$ and $\psi_2$ are the azimuth angle of the left, respectively the right edge of the window relative to the point of reference P (in radians)
- $\psi_{sw}$ is the solar azimuth relative to the azimuth angle of the window normal $\psi_s - \psi_w$, where $\psi_w$ is the azimuth angle of the window normal (in radians, from south to west).

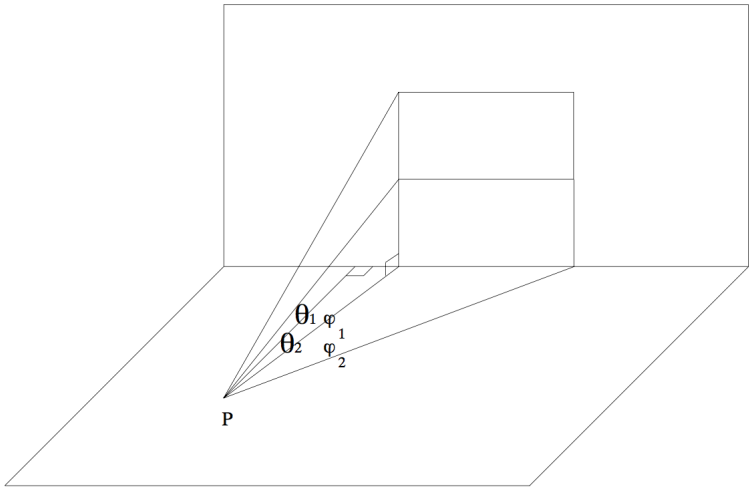


Figure 3.3: The altitude and the azimuth angles of the edges of the window, seen by the point of reference P inside the room (illustration from [3])

The corresponding angles are shown in Figure 3.3. If these conditions are fulfilled, the beam illuminance can be computed by the following expression:

$$E_{r,b} = \tau_w(\theta_i)E_b$$

where $\tau_w(\theta_i)$ corresponds to the light transmittance of the window with the angle of incident $\theta_i$ [3]. $E_b$ is the horizontal beam illuminance measured outdoors. To calculate the light transmittance of the window, in general the approximation of Rivero is used [3]:

$$\tau_w(\theta_i) = 1.018\tau_w(0)\cos(\theta_i)(1 + \sin^3(\theta_i))$$

The interior horizontal diffuse illuminance does not depend on direct sunlight exposure, but it considers the sky luminance and the solid angle of the window seen by the point P [3]. It can be calculated using the following equation [3]:

$$E_{r,d} = \frac{\tau_w L}{2}\{\frac{z}{\sqrt{h_p^2 + z^2}}(\arctan\frac{x_w + w_w - x_p}{\sqrt{h_p^2 + z^2}} + \arctan\frac{x_p - x_w}{\sqrt{h_p^2 + z^2}}) - \frac{z}{\sqrt{(h_p + h_w)^2 + z^2}}(\arctan\frac{x_w + w_w - x_w}{\sqrt{(h_p + h_w)^2 + z^2}} + \arctan\frac{x_p - x_w}{\sqrt{(h_p + h_w)^2 + z^2}})\}$$

where

- $L$ Luminance of radiating surface ($cd/m^2$)
- $z$ Perpendicular distance from the window ($m$)

- $h_p$ Height of the lower edge of the window and the plane of reference $(m)$
- $h_w$ Height of window $(m)$
- $x_p$ Distance between the reference point P and the left wall $(m)$
- $x_w$ Distance between the left edge of the window and the left wall $(m)$
- $w_w$ Width of the window $(m)$

In this work, the reflected illuminance is assumed to contribute a negligible amount to the total energy, compared to the diffuse and beam illuminance, and is therefore neglected. Consequently, the total illuminance is viewed as the sum of the beam and diffuse illuminance:

$$E_v = \tau_w(\theta_i)E_b + \frac{\tau_w L}{2}\{\frac{z}{\sqrt{h_p^2+z^2}}(\arctan\frac{x_w+w_w-x_p}{\sqrt{h_p^2+z^2}} + \arctan\frac{x_p-x_w}{\sqrt{h_p^2+z^2}})- \frac{z}{\sqrt{(h_p+h_w)^2+z^2}}(\arctan\frac{x_w+w_w-x_w}{\sqrt{(h_p+h_w)^2+z^2}} + \arctan\frac{x_p-x_w}{\sqrt{(h_p+h_w)^2+z^2}})\}$$

As the filtering of windows is generally optimized to $V(\lambda)$ [4], it is assumed that only a negligible amount of ultraviolet and infrared light enters the room. Therefore, the interior illuminance distribution, which corresponds to the visible band of the solar spectrum, is the only component that provides harvestable energy.

## 3.3 Energy model

This section addresses the second part of the analytical model, which targets the conversion of illuminance to energy. The derivation of the model and its components are explained and discussed.

### 3.3.1 Derivation of the model

The energy model is divided into three steps. First, the illuminance is converted into luminous flux by using the fact, that the luminous flux is the product of the illuminance and the receiving surface. In the second step, the luminous flux is translated to radiant flux by dividing the luminous flux through the maximum radiation luminous efficacy. To convert radiant power into energy, the computed power is multiplied by the time. Each step is explained in more detail in the following passages.

1. The beginning of the derivation is set by the estimation of the luminous flux $\Phi_v$. It corresponds by definition to the received illuminance $E_v$ times the receiving area $A$:
$$\Phi_v = E_v * A$$

2. In a next step, the luminous flux $\Phi_v$ is converted into radiant flux $\Phi_e$. To calculate the luminous flux, the luminous efficacy of radiation $K$ is used. It measures the amount of electromagnetic power that can be used for lighting:
$$K = \frac{\Phi_v}{\Phi_e}$$
As in this thesis it is assumed that all light entering a location contributes electromagnetic energy and can be used for lighting, the luminous efficacy is set to the maximum value: $K_m = 683.002\ lm/W$. Therefore, the radiant flux can be computed by dividing the luminous flux $\Phi_v$ by the maximum luminous efficacy of radiation $K_m$:
$$\Phi_e = \frac{\Phi_v}{K_m} = \frac{E_v * A}{K_m}$$

3. To compute the energy, one last step is performed. As the radiant flux $\Phi_e$ is defined by the radiant energy $E_{in}$ emitted or received, per unit time $t$, the energy can be estimated by multiplying the radiant power $\Phi_v$ by the time $t$:
$$E_{in} = \Phi_e * t = \frac{\Phi_v * t}{K_m} = \frac{E_v * A * t}{K_m}$$
To account for the lost power due to the conversion of solar energy to electrical energy, the previous expression is multiplied by the solar panel efficiency parameter $\mu$:
$$E_{in} = \frac{E_v * A * \mu * t}{K_m}$$

Chapter 4

# Model evaluation

In this chapter, first steps towards evaluating the analytical model are presented. The beam illuminance and energy model are discussed.

## 4.1 Beam illuminance evaluation

This section addresses the beam illuminance model. It is a model that assesses whether the condition for beam illuminance, which is introduced in 3.2, is satisfied. The input of the model are the solar altitude and azimuth angles as well as the azimuth angle of the window normal. The output is set to "False" in case of no direct sunlight and set to "True" in case of a beam illuminance contribution. The following subsections explain the general setup and verify the model's performance by comparing the estimated direct sunlight condition to measured data.

### 4.1.1 Setup

In order to evaluate the beam illuminance model, a data set provided by the Computer Engineering Group ETH Zurich, is used which contained measurements of indoor illuminance and harvested energy [10]. For the beam illuminance evaluation, location 2 (location 14 in [10]) is considered. The measured room and window geometries are shown in Table 4.1. The solar energy harvesting device which was used to measure the illuminance and harvested energy, is placed at the left wall at a height of $2.1m$, $1.3m$ away from the window.
For the evaluation, the time horizon between the 25th and the 31st of May of the year 2020 is considered and the corresponding solar altitude and azimuth angles for location 2 (47.3778°N, 8.5523°E) are calculated.
To assess whether a point of reference P is hit by direct sunlight, given a clear sky, the following two conditions must be satisfied [3]:

$$\theta_1 < \theta_s < \theta_2 \quad \text{and} \quad \psi_1 < \psi_{sw} < \psi_2$$

| Measured room and window geometry of location 2 | $m$ |
|---|---|
| Length of the room | 10 |
| Width of the room | 3.72 |
| Height of the room | 2.7 |
| Width of the window | 3 |
| Height of the window | 1.62 |
| Distance between left wall and left edge of window | 0.36 |
| Distance between right wall and right edge of window | 0.36 |
| Distance between ground to lower edge of the window | 0.78 |

Table 4.1: Room and window geometries of location 14

The angles $\theta_1$, $\theta_2$, $\psi_1$, and $\psi_2$ are calculated through the room and window geometries in respect to the position of the solar harvesting device. Next, the condition is examined in a time interval of one hour and compared to the measured illuminance. If the condition is fulfilled, the beam condition is set to "True", if not it is set to "False". The result is compared to the measured illuminance.

### 4.1.2 Evaluation

It is expected that in case of direct sunlight, the measured illuminance is higher compared to other times of the measurement horizon. As the beam condition returns "True" in case of beam illuminance, it can be assumed that the condition correlates with the measured illuminance peak occurrences. For the evaluation of the beam illuminance model, the measured indoor illuminance is visually compared to the expected beam illuminance occurrence.
In Figure 4.1 two main things can be observed. First of all, on six of the seven considered dates a big illuminance peak can be seen. These six illuminance peaks align well with the evaluated beam illuminance condition. A strong correlation from the direct sunlight condition being true to a considerably bigger amount of harvestable energy can be detected. As a consequence, it makes sense to estimate a position with considerable direct sunlight exposure to place a solar harvesting device, in order to harvest more energy. In conclusion, beam illuminance does not always play a role but when it does a significantly high energy contribution can be seen which would be intuitively expected with direct sunlight.
Secondly, the direct sunlight condition applied to the data set matches the peaks in all but a single case. On the day where the model does not perform according to the measurements no peak is detected, yet the beam illuminance model suggests that a peak should occur. Since the days before and after this date show a peak and the sun movement was minimal, it is reasonable to assume this off value is due to weather conditions, such as an overcasted sky or other external factors.

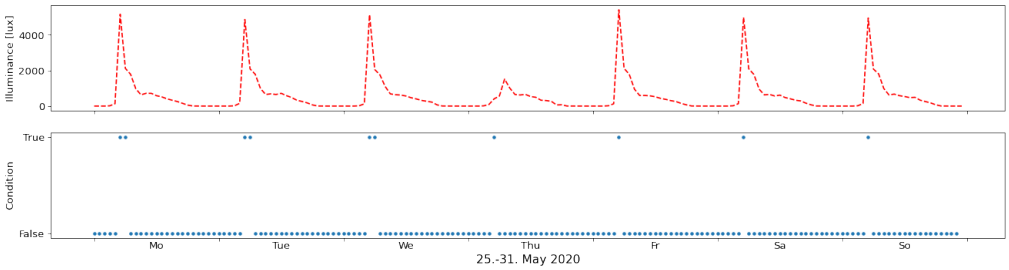


Figure 4.1: Measured illuminance (top) versus calculated beam condition (bottom).

## 4.2 Energy model evaluation

In this section, the performance of the energy model is evaluated. By applying the model on a data set [10] of measured illuminance, the computed energy is compared to the measured energy values. Five samples of two different locations (location 06 and location 14 in [10]) are considered and for visual comparison the results are plotted.

### 4.2.1 Setup

To evaluate the model, a data set [10] provided by the Computer Engineering Group ETH Zurich is used which contains the measured illuminance $E_v$ and harvested energy $E_{in}$ of a solar panel device deployed at two different locations at ETH Zurich. The data set contains three years of measurements of location 1 (location 06 in [10]) and one year of measurement of location 2 (location 14 in [10]). For the evaluation, five samples of different time horizons were considered, one sample of each season and additionally a week from May.
To assess the performance of the derived energy model, the parameter $A_{solar}$ [10] is set to the solar panels size, which was used during the measurement: $A_{solar} = 0.00165m^2$. For the efficiency $\mu_{solar}$, a general estimation of solar panel efficiencies is assumed and therefore set to $\mu_{solar} = 0.2$. $K_m$ is the maximum radiation luminous efficacy and therefore of value 683.002 $lm/W$. To calculate the energy of an hour, $t$ is set to $3600s$.
After defining all parameters, the measured illuminance values $E_v$ are plugged into to model and $E_{in}$ is calculated. The computed output is visually compared to the measured harvested energy through several plots.

### 4.2.2 Evaluation

The evaluation shows that the model performs well in both locations. Especially in the first location, the model performs accurately over the whole time horizon

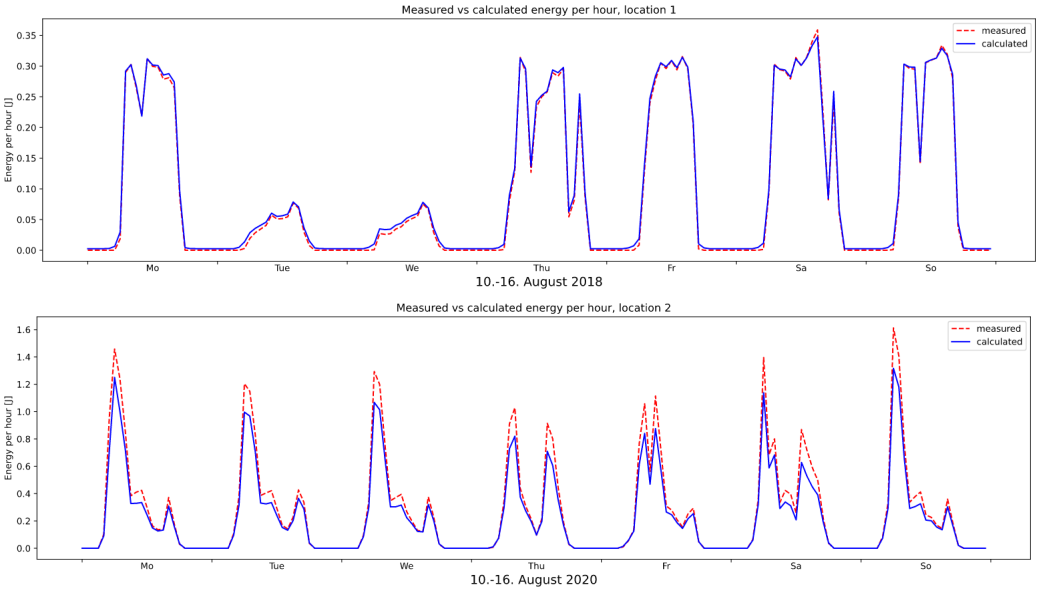


Figure 4.2: Measured versus calculated energy compared in two different locations during summer 2018 (top) and 2020 (bottom).

and tends to slightly underestimate the harvestable energy only in the peaks. In the second location, the model also performs reasonably well but during the energy peaks it tends to be significantly off by an average factor of two. It can be observed that location 2 harvests considerably more energy than location 1. Especially the month May (Figure 4.6) shows an amount of harvested energy which is multiple times bigger compared to the four other samples. During the peaks of the summer (Figure 4.2), fall (Figure 4.3), winter (Figure 4.4), and spring (4.5) the measured energy peak never exceeds $1.7J$ in an hour while in the sample of May (Figure 4.6) six out of seven days harvest over $14J$ during their energy peak hour. On the date which does not show such a high peak in energy, the maximum still lies over $3J$. This indicates that the range of harvestable energy varies strongly over the day and year, resulting in a significantly higher amount of harvestable energy in specific cases.
It can be concluded that the energy model performs very well in the first location which never exceeds $0.4J$ of harvested energy in its energy peak hours. The model tends to slightly underestimate the peak values of harvestable energy which could be due to inaccuracies during measurements.
In the case of the second room, the model still performs reasonably well but tends to underestimate the harvestable energy during the energy peaks by an average factor of two in the worst case (Figure 4.6). Again, this could be due to inaccuracies during measurements.

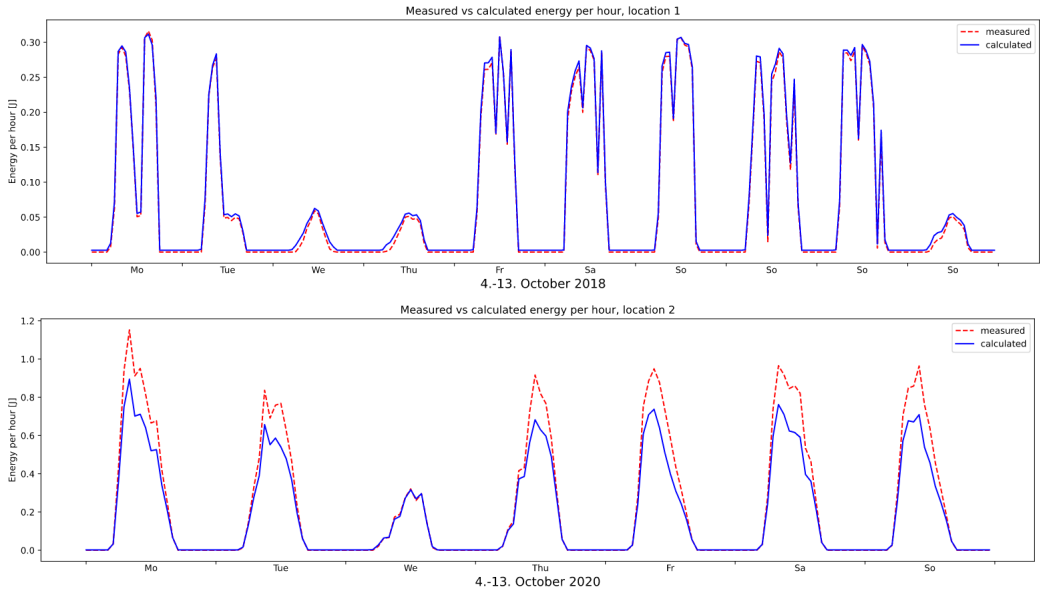


Figure 4.3: Measured versus calculated energy compared in two different locations during fall 2018 (top) and 2020 (bottom).

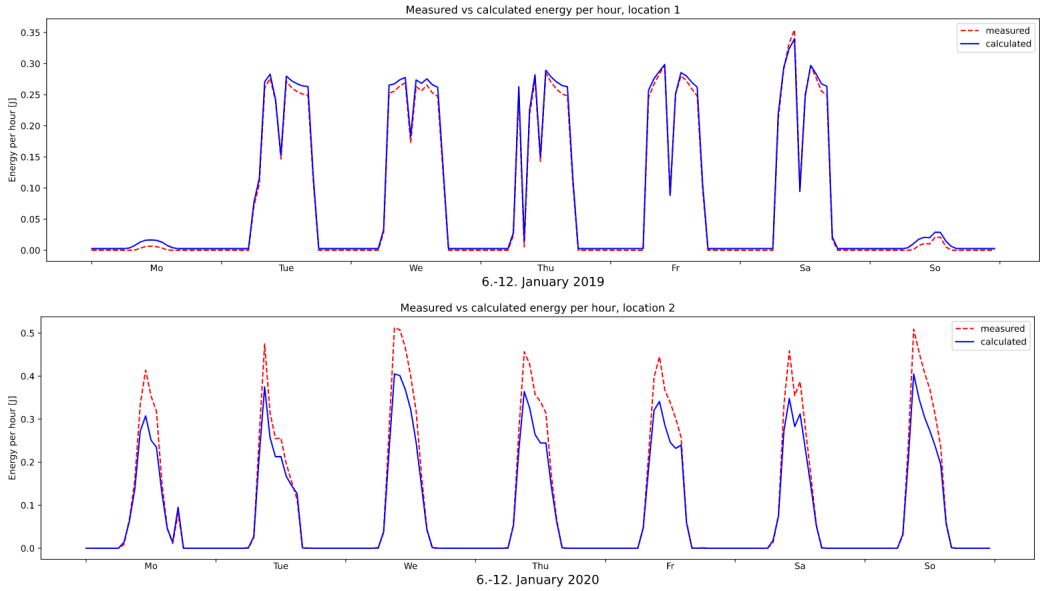


Figure 4.4: Measured versus calculated energy compared in two different locations during winter 2019 (top) and 2020 (bottom).

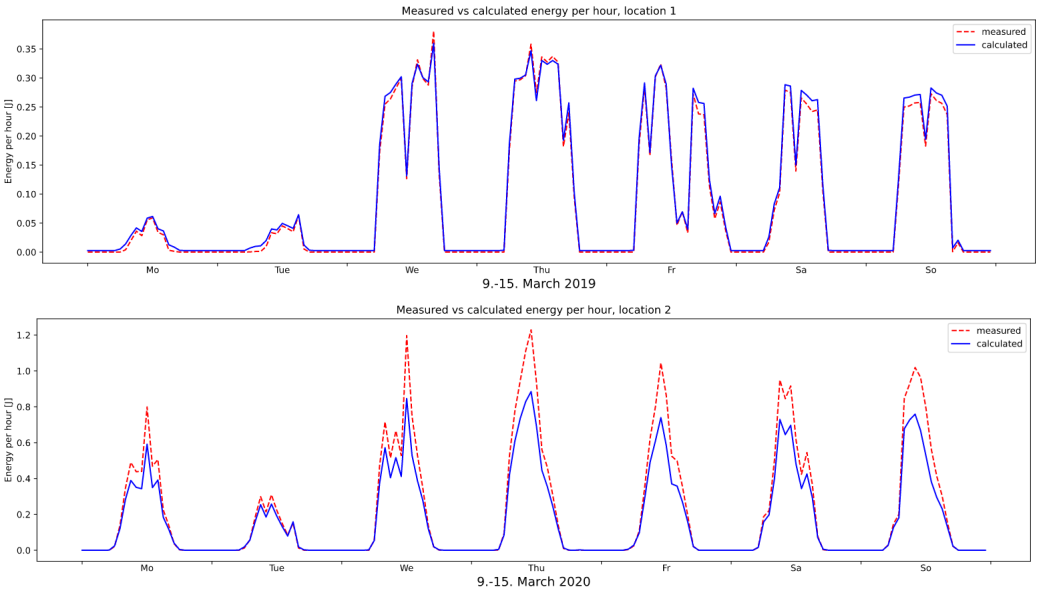


Figure 4.5: Measured versus calculated energy compared in two different locations during spring 2019 (top) and 2020 (bottom).

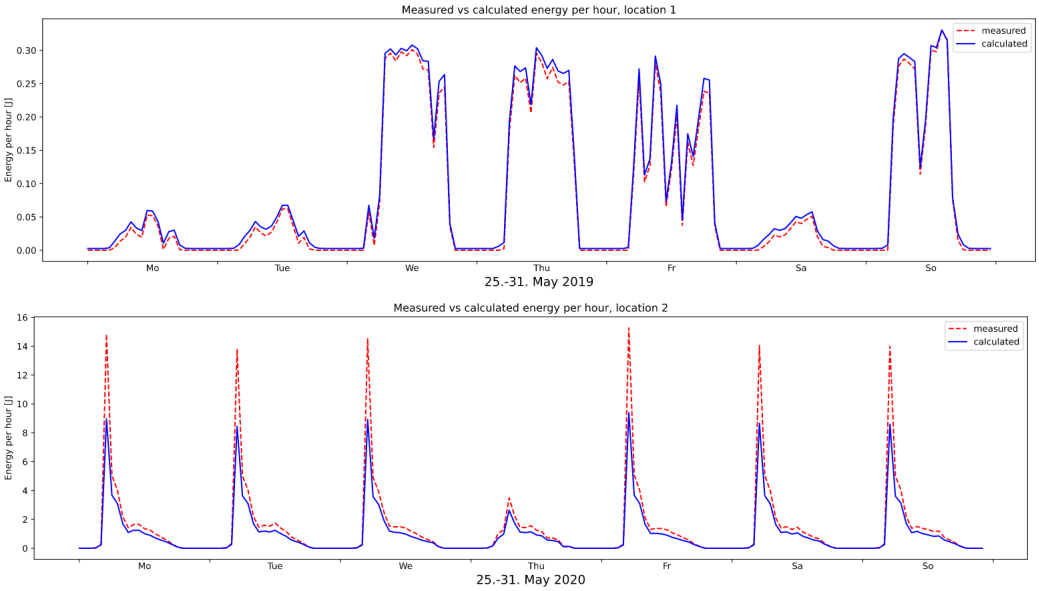


Figure 4.6: Measured versus calculated energy compared in two different locations during May 2019 (top) and 2020 (bottom).

Chapter 5

# Deployment of indoor solar harvesting devices

In the previous chapter, two different locations were examined, and the considerable variation of harvested energy was discussed. As it was concluded that more harvestable energy is provided in case of direct sunlight exposure, a reasonable strategy to maximize energy harvesting lies in the determination of the position with the most exposure to beam illuminance. Taking this into account, a deployment model is introduced which, based on window coordinates and the sun movement, computes the number of hours of direct sunlight hours at each point in a room. This model can be used to calculate the total number of beam illuminance hours in an empty indoor location. As a consequence, it can assist in determining suitable deployment positions of a solar harvesting device.

## 5.1 Deployment location evaluation

In this section, the setup of the deployment model is presented and furthermore, its evaluation for five different cases is discussed.

### 5.1.1 Setup

The evaluated room, which corresponds to location 2 from the previous chapter (location 14 in [10]), is located at ETH Zurich (47.3778°N, 8.5523°E) and contains one window facing North-East. The room and window geometries are listed in Table 4.1. The data collected at this location shows that the room is occasionally exposed to beam illuminance. For the evaluation, a time horizon of 24 hours of the 25.05.2020 is considered.
The deployment model utilizes the room geometry and solar altitude as well as azimuth angles to calculate the beam illuminance hours. Furthermore, the coordinates of the window corners are considered. These points consist of three

coordinates of which $x$ represents the room length, $y$ stands for the width of the room and $z$ corresponds to the height. Furthermore, the solar altitude and azimuth angles of each hour are determined in radians, as well as the azimuth angle of the window normal from south to west, which in this case is $\psi_w = 48°$. To compare different areas in a room, the model evaluates a grid of potential solar energy harvesting device deployment positions. For each of these, the model first calculates the relevant angles for the beam illuminance condition and then verifies the condition for each hour of the considered time horizon. In a last step, the total number of beam illuminance hours are summed up at each point. Five different cases are illustrated through heatmaps which show the beam illuminance hour distribution inside location 2.
The deployment evaluation model considers an ideal scenario based on three simplifications. The model assumes a clear sky and an empty room, as clouds or furniture would decrease the amount of direct sunlight through blocking direct sun rays. Furthermore, it is supposed that no buildings and trees are standing between the window and the sun, as this would additionally block beam illuminance from entering the window.

### 5.1.2 Evaluation

For the evaluation of the deployment model, five heatmaps are plotted to visualize the beam illuminance hour distribution for a day in May. As not all positions are suited for a solar energy harvesting device placement, only five potential areas are considered.
The first three Figures, 5.1, 5.2, 5.3, show the direct sunlight hour distribution at ground height of location 2 ($z = 0.0m$), at average desk height ($z = 0.7m$), as well as at shelf height ($z = 2.0m$) to compare different heights for deployment. The fourth Figure, 5.4, shows the left ($y = 0.0m$) and the right wall ($y = 3.70m$) to determine, whether the beam illuminance hour differs in these cases.
In Figure 5.1 the beam illuminance hour distribution of the ground height is plotted. It can be observed that the highest number of beam illuminance hours is computed below the left half of the window and corresponds to eleven beam illuminance hours. However, the amount of beam illuminance hours varies below the window itself. The right half below the window counts only five beam illuminance hours at its minimum. Furthermore, it can be seen that no sunlight reaches the corners of the room and that the amount of beam illuminance hours decreases when moving to the back of the room. The pattern of the beam illuminance hour distribution suggests that the sun rises above the top right corner of the plot and proceeds to advance to the right. Because of the movement of the sun, the determined distributions make sense. Even though the number of beam illuminance hours is high below the window, the floor is generally not a suitable place for a measurement device. Workplaces are often located at the window which could block direct sun rays, or the device could potentially be harmed.

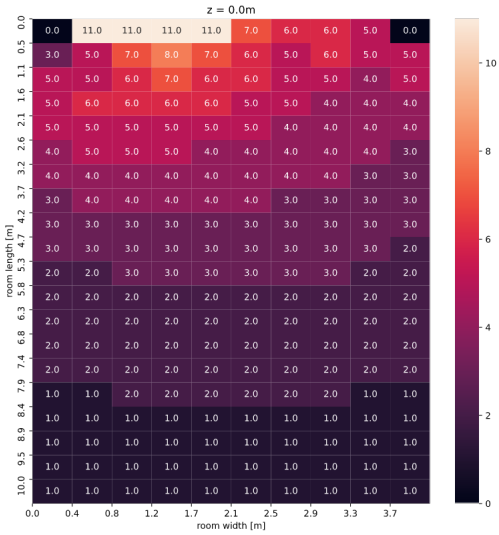


Figure 5.1: Beam illuminance hours distribution calculated for ground height.

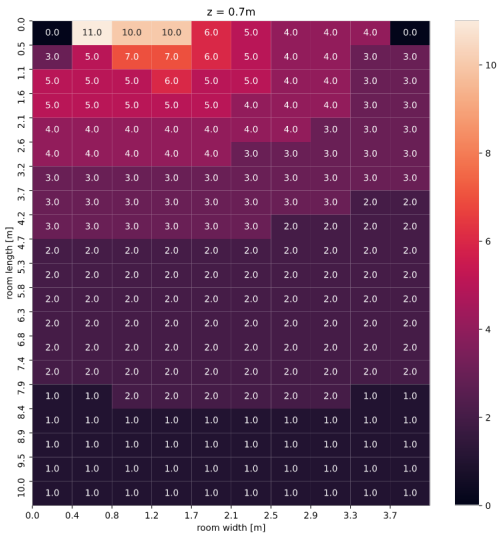


Figure 5.2: Beam illuminance hours distribution calculated for desk height.

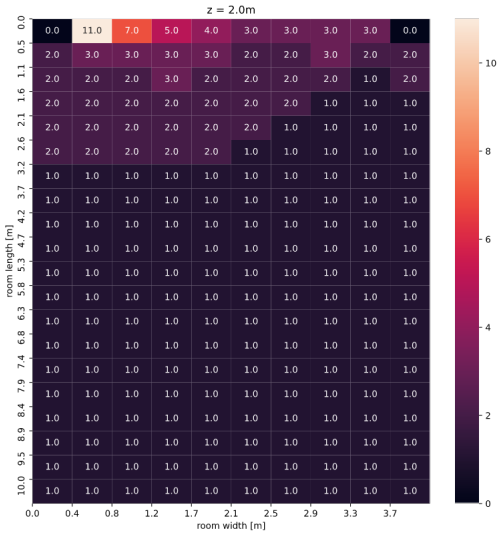

| | 0.0 | 0.4 | 0.8 | 1.2 | 1.7 | 2.1 | 2.5 | 2.9 | 3.3 | 3.7 |
|---|---|---|---|---|---|---|---|---|---|---|
| 0.0 | 0.0 | 11.0 | 7.0 | 5.0 | 4.0 | 3.0 | 3.0 | 3.0 | 3.0 | 0.0 |
| 0.5 | 2.0 | 3.0 | 3.0 | 3.0 | 3.0 | 2.0 | 2.0 | 3.0 | 2.0 | 2.0 |
| 1.1 | 2.0 | 2.0 | 2.0 | 3.0 | 2.0 | 2.0 | 2.0 | 2.0 | 1.0 | 2.0 |
| 1.6 | 2.0 | 2.0 | 2.0 | 2.0 | 2.0 | 2.0 | 2.0 | 1.0 | 1.0 | 1.0 |
| 2.1 | 2.0 | 2.0 | 2.0 | 2.0 | 2.0 | 2.0 | 1.0 | 1.0 | 1.0 | 1.0 |
| 2.6 | 2.0 | 2.0 | 2.0 | 2.0 | 2.0 | 1.0 | 1.0 | 1.0 | 1.0 | 1.0 |
| 3.2 | 1.0 | 1.0 | 1.0 | 1.0 | 1.0 | 1.0 | 1.0 | 1.0 | 1.0 | 1.0 |
| 3.7 | 1.0 | 1.0 | 1.0 | 1.0 | 1.0 | 1.0 | 1.0 | 1.0 | 1.0 | 1.0 |
| 4.2 | 1.0 | 1.0 | 1.0 | 1.0 | 1.0 | 1.0 | 1.0 | 1.0 | 1.0 | 1.0 |
| 4.7 | 1.0 | 1.0 | 1.0 | 1.0 | 1.0 | 1.0 | 1.0 | 1.0 | 1.0 | 1.0 |
| 5.3 | 1.0 | 1.0 | 1.0 | 1.0 | 1.0 | 1.0 | 1.0 | 1.0 | 1.0 | 1.0 |
| 5.8 | 1.0 | 1.0 | 1.0 | 1.0 | 1.0 | 1.0 | 1.0 | 1.0 | 1.0 | 1.0 |
| 6.3 | 1.0 | 1.0 | 1.0 | 1.0 | 1.0 | 1.0 | 1.0 | 1.0 | 1.0 | 1.0 |
| 6.8 | 1.0 | 1.0 | 1.0 | 1.0 | 1.0 | 1.0 | 1.0 | 1.0 | 1.0 | 1.0 |
| 7.4 | 1.0 | 1.0 | 1.0 | 1.0 | 1.0 | 1.0 | 1.0 | 1.0 | 1.0 | 1.0 |
| 7.9 | 1.0 | 1.0 | 1.0 | 1.0 | 1.0 | 1.0 | 1.0 | 1.0 | 1.0 | 1.0 |
| 8.4 | 1.0 | 1.0 | 1.0 | 1.0 | 1.0 | 1.0 | 1.0 | 1.0 | 1.0 | 1.0 |
| 8.9 | 1.0 | 1.0 | 1.0 | 1.0 | 1.0 | 1.0 | 1.0 | 1.0 | 1.0 | 1.0 |
| 9.5 | 1.0 | 1.0 | 1.0 | 1.0 | 1.0 | 1.0 | 1.0 | 1.0 | 1.0 | 1.0 |
| 10.0 | 1.0 | 1.0 | 1.0 | 1.0 | 1.0 | 1.0 | 1.0 | 1.0 | 1.0 | 1.0 |

Figure 5.3: Beam illuminance hours distribution calculated for shelf height.

Figure 5.2 shows the beam illuminance hour distribution at desk height. The amount of direct sunlight is highest around the window and again its maximum corresponds to eleven beam illuminance hours. However, compared to Figure 5.1, there is only one position with so many beam illuminance hours and the right side of the window computes even less beam illuminance hours compared to the floor case, which is only four beam illuminance hours. This could be due to a steep angle inclination of the sun towards the window, which results in more direct sunlight exposure of the floor below the window compared to the area at desk height. The corners next to the window are again not exposed to beam illuminance at all. Again, because of the movement of the sun, the determined distributions make sense.

Figure 5.3 shows the number of beam illuminance hours at shelf height. It can be observed that in this case nearly no direct sunlight is computed, except for a few positions in the top left corner at the top of the window, where again a maximum number of eleven beam illuminance hours is calculated. In this case, the difference between the right side of the top of the window and the left side is bigger than in the previous two cases. The smallest amount of beam illuminance hours at the right side of the top corresponds to only three hours. The corners next to the window are still the only positions which receive zero beam illuminance hours and even though nearly the whole room is exposed to only one beam illuminance hour, the same beam illuminance hour distribution shift to the left side of the room as before can be recognized.

The fact that there is still a spot which can harvest the same amount of maximum beam illuminance hours, like the ground and desk height case, demonstrates that different areas can have positions of similar potential regarding maximum energy

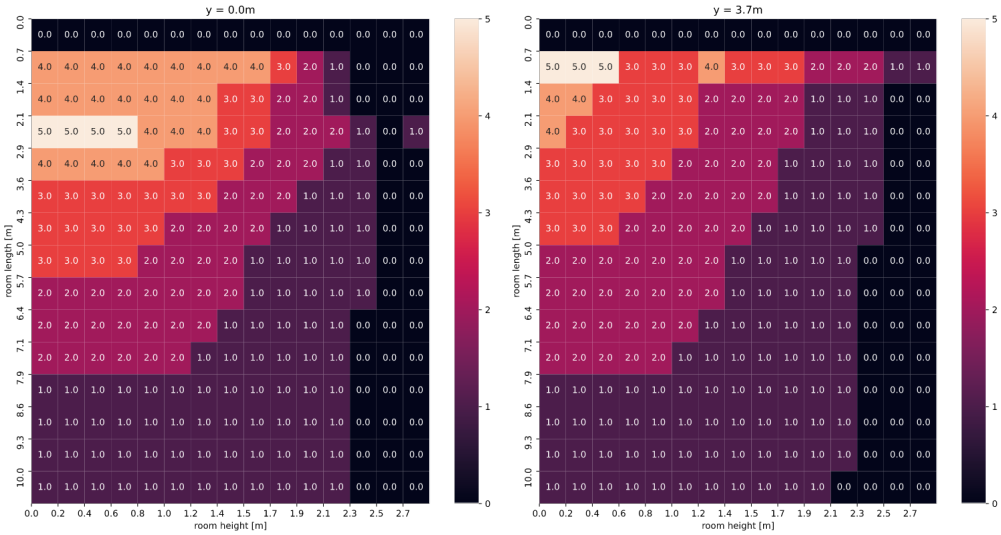


Figure 5.4: Beam illuminance hours distribution for left wall (left) and right wall (right)

supply.

In Figure 5.4, the heatmaps of the right and left wall of location 2 are plotted. It can be observed that compared to the previous considered cases, the maximum beam illuminance hour corresponds now to five instead of eleven hours in both cases. However, the lines at the top which correspond to the corners next to the window are still receiving no direct sunlight. Furthermore, again a shift of the beam illuminance hour distribution can be observed. In this case, the distribution is shifted downwards and away from the window. This makes intuitively sense, as the sun rises higher over the day and therefore more sun rays are getting blocked by the top of the window.
Comparing the two walls, it can be seen that the left wall is generally more exposed to direct sunlight than the right one. Moreover, the maximum number of beam illuminance hours are found further away from the window compared to the right wall, where they are found right next to the corner. Because of the rising position and movement of the sun, it makes sense that the left wall is more exposed to direct sunlight. Lastly, it can be observed, that except for a few points, no beam illuminance hours are computed for the top of the room. Due to the inclination angles of the sun this observation is reasonable.
It can be concluded that, regarding deployment height, solar energy harvesting devices are able to harvest more energy when they are placed nearby a window. Nevertheless, the amount of beam illuminance hours varies highly around the window itself which is observed at ground, desk and shelf height. As the height increases, the variation along the window length increases as well. Furthermore, a beam illuminance hour distribution shift is observed, which corresponds to the

movement of the sun.
In case the solar panel should be placed on a wall, it is important to consider, that the maximum number of beam illuminance hour might be significantly smaller compared to positions at the window itself. Furthermore, the highest number of beam illuminance hours is not found at the positions closest to the window. The corners next to the window are not exposed to direct sunlight at all and in case of the left wall the maximum number of beam illuminance hours is shifted to the back of the room. The reason for this shift can again be found in the movement of the sun. As the rising position of the sun also changes over the year, the observed heatmap would change significantly in terms of beam illuminance hour distribution pattern and maximum beam illuminance hours.

Chapter 6

# Outlook

Considering the performance of the energy formula in the evaluated locations, a varying accuracy can be observed in terms of the energy peaks. Through further analysis on the energy behaviour during beam illuminance exposure, it could be investigated whether the underestimation is due to crude parameter estimation or whether other factors play a role. If this is the case, the energy model should be adapted to provide a precise model in general and not exclusively in cases where only a small amount of energy is harvested compared to other locations.
To achieve a reliable overall performance, in addition to the energy model, all components of the analytical model need to be extensively evaluated. In particular, the illuminance model needs additional validation.
To determine the ideal placement of a solar energy device and to compute the harvestable energy at that location, the deployment location evaluation needs to be complemented by an energy calculation. The deployment model itself can provide a clearer insight on the beam illuminance evolution, if the condition is verified for more iterations in terms of sun angles. Instead of considering an hourly change in the sun's positioning, examining the beam illuminance values per minute at each point is a reasonable range. On the other hand, a deployment evaluation over a longer period of time needs to be inspected to draw conclusions of the accuracy of the model regarding long term usage.

Chapter 7

# Conclusion

This work presents an analytical model to determine the harvestable energy in an indoor location from natural light sources, and a deployment model for indoor solar harvesting devices. Two parts of the analytical model are evaluated. The beam illuminance model demonstrates a high correlation between the beam illuminance condition and measured illuminance peaks for the evaluated location. The energy model performs well in both considered locations but varies in its accuracy regarding energy peak values. The deployment model is evaluated for three different potential deployment heights and two walls at a specific location at ETH Zurich. The resulting beam illuminance hour distributions align with the movement of the sun.

# Bibliography


[1] Bernhard Buchli, Felix Sutton, Jan Beutel, and Lothar Thiele. Towards enabling uninterrupted long-term operation of solar energy harvesting embedded systems. In Bhaskar Krishnamachari, Amy L. Murphy, and Niki Trigoni, editors, *Wireless Sensor Networks*, pages 66–83, Cham, 2014. Springer International Publishing.

[2] Chul-Ho Kim and Kang-Soo Kim. Development of sky luminance and daylight illuminance prediction methods for lighting energy saving in office buildings. *Energies*, 12(4), 2019. ISSN 1996-1073. URL `https://www.mdpi.com/1996-1073/12/4/592`.

[3] E. Vartiainen. Daylight modelling with the simulation tool delight. 2000.

[4] Fondriest environmental, inc. "solar radiation and photosynethically active radiation." fundamentals of environmental measurements. `https://www.fondriest.com/environmental-measurements/parameters/weather/solar-radiation/`, 3 2014. Accessed: 2021-02-26.

[5] Asim Kumar Roy Choudhury. 1 - characteristics of light sources. In Asim Kumar Roy Choudhury, editor, *Principles of Colour and Appearance Measurement*, pages 1–52. Woodhead Publishing, 2014. ISBN 978-0-85709-229-8. doi: https://doi.org/10.1533/9780857099242.1. URL `https://www.sciencedirect.com/science/article/pii/B9780857092298500012`.

[6] Lindsay T. Sharpe, Andrew Stockman, Wolfgang Jagla, and Herbert Jägle. A luminous efficiency function, V*($\lambda$), for daylight adaptation. *Journal of Vision*, 5(11):3–3, 12 2005. ISSN 1534-7362. doi: 10.1167/5.11.3. URL `https://doi.org/10.1167/5.11.3`.

[7] M. Cucumo, A. De Rosa, V. Ferraro, D. Kaliakatsos, and V. Marinelli. Correlations of global and diffuse solar luminous efficacy for all sky conditions and comparisons with experimental data of five localities. *Renewable Energy*, 33(9):2036–2047, 2008. ISSN 0960-1481. doi: https://doi.org/10.1016/j.renene.2007.11.015. URL `https://www.sciencedirect.com/science/article/pii/S0960148107003801`.

[8] Su-In Yun and Kang-Soo Kim. Sky luminance measurements using ccd camera and comparisons with calculation models for predicting indoor illuminance. *Sustainability*, 10:1556, 05 2018. doi: 10.3390/su10051556.

[9] Xinyu Ma, Sebastian Bader, and Bengt Oelmann. Estimating harvestable energy in time-varying indoor light conditions. ENSsys '20, page 71–76, New York, NY, USA, 2020. Association for Computing Machinery. ISBN 9781450381291. doi: 10.1145/3417308.3430270. URL `https://doi.org/10.1145/3417308.3430270`.

[10] Lukas Sigrist, Andres Gomez, and Lothar Thiele. Long-term tracing of indoor solar harvesting. Zenodo, March 2020. doi: 10.5281/zenodo.3715472. URL `https://doi.org/10.5281/zenodo.3715472`. Appears in the Proceedings of the 2nd Workshop on Data Acquisition To Analysis (DATA '19).